Intergranular Interactions and Thermal Stability in Fe–Ti–N Thin Films

Kumar Srinivasan, C. Scott Brown, Jaydip Das, and Carl E. Patton

Department of Physics, Colorado State University, Fort Collins, CO 80523 USA

Intergranular interactions and thermal stability factors in Fe–Ti–N thin films were studied as a function of nitrogen content. This was done through: 1) measurements of the isothermal remanence magnetization and direct current demagnetization, coupled with an analysis based on a modified Che–Bertram interaction field model for the intergranular interactions and 2) measurements of the dependence of the coercive force on the holding time for the applied field, coupled with a Sharrock analysis in the case of the thermal stability. The data indicate that the intergranular interactions are mainly exchange dominated for nitrogen levels in the 0–4 at.% range, become primarily magnetostatic for 4–7 at.% nitrogen, and switch back to exchange dominated for higher levels. For nitrogen amounts in the 7–11 at.% range, the thermal stability factors are largest at about 7 at.% and decrease for higher nitrogen amounts. The inferred unit switching lateral size from the Sharrock analysis is about 10–20 times larger than the grain size. The changes in the intergranular interactions and the thermal stability factors with nitrogen content can be qualitatively explained by a grain size effect.

Index Terms—**Fe–Ti–N thin films, intergranular interactions, thermal stability.**

I. Introduction

SOFT magnetic Fe–Ti–N thin films with high magnetization, a low coercive force, low loss, and a well defined in-plane uniaxial anisotropy are promising candidates for use as soft magnetic elements for perpendicular recording magnetic recording heads [1], [2]. Based on work on other metallic ferromagnetic films for low-loss field-tunable band-stop filters [3], [4] such films are also likely to find applications in metallic film based microwave devices. Recent work on the role of nitrogen in Fe–Ti–N films includes studies of the thermal stability of the anisotropy [5], changes in crystal structure [6], [7], microstructure, and microwave loss [8], [9].

All of these properties are of practical importance in both recording and high-frequency applications. They ultimately relate, moreover, to the type and extent of the magnetic interactions between the grains and the thermal stability of the grains. The magnetic interactions, for example, can influence the magnetization reversal modes and contribute to undesirable read-out noise in magnetic recording. When magnetic moments flip due to thermal instability, they introduce an additional source of noise that deteriorates the recording performance. This work reports on the analysis of the intergranular (IG) interactions, thermal stability, and effective switching volumes in the Fe–Ti–N system as a function of nitrogen content (x_N). Intergranular interactions were studied by means of isothermal remanence (IRM) and direct current demagnetization (DCD) measurements [10]. The analysis was based on a modified Che–Bertram interaction field model [11]–[13]. The thermal stability factors and switching volumes were determined through a Sharrock analysis of the dynamic coercivity [14], [15].

For nitrogen amounts in the 0–4 at.% range, intergranular exchange interactions are dominant. For 4–7 at.% nitrogen, the interactions are primarily magnetostatic. For higher levels of nitrogen, the interactions are again dominated by exchange. The change in the intergranular interactions from exchange dominated to magnetostatic dominated and back again can be qualitatively explained in terms of the decrease in grain size, microstructure development, and exchange length considerations. Thermal stability parameters and effective switching volumes could only be determined for nitrogen amounts in the 7–11 at.% range. The thermal stability factors appear to decrease slightly as the nitrogen level is increased and the grain size decreases. However, the switching volumes from the Sharrock analysis have lateral dimensions that appear to be 10–20 times larger than the grain sizes. For $x_N, < 7$ at.%, the changes in the coercive force with the field holding time were too small for meaningful measurements.

Section II explains the IRM and DCD measurement schemes, the extended Che–Bertram remanence mean field approach to IG interactions, and the Sharrock dynamic coercive force model for the analysis of thermal stability and switching volume determinations. Section III describes the Fe–Ti–N thin film materials, and summarizes the microstructural and static magnetic properties. Data on intergranular interactions and the interaction field based analysis of the data are presented in Section IV-A. Section IV-B gives results on the thermal stability and switching volume analysis. Section V gives a summary and conclusion.

II. Interactions and Thermal Stability Analysis

A. IRM and DCD Remanence Parameters and the Interaction Field Analysis Technique

Fig. 1 gives a schematic view of the IRM and DCD measurement procedures. For an individual IRM determination, one starts with a demagnetized sample at point A, cycles the field H from zero to some stopping field $H_{\rm stop}$ and back to zero, and then measures the isothermal remanence magnetization (IRM) $M_{\rm IRM}$. The DCD remanence is obtained if one starts at the standard remanence point B, labeled as M_R in the diagram, cycles the field to some $-H_{\rm stop}$ and back to zero, and then measures $M_{\rm DCD}$.

One generally makes both measurements for a full range of $H_{\rm stop}$ values. For purposes of analysis, it proves convenient to normalize all of the remanence data to M_R and all of the field values to the coercive force. Such reduced remanence values will be denoted by a lower case $m_{\rm IRM}$ or $m_{\rm DCD}$, as needed. The

Digital Object Identifier 10.1109/TMAG.2007.900691

0018-9464/$25.00 © 2007 IEEE

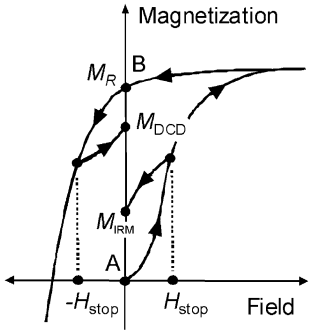

Fig. 1. Schematic magnetization versus field diagram that shows the isothermal remanence magnetization $M_{\rm IRM}$ and direct current demagnetization remanence $M_{\rm DCD}$ measurement procedures for a stopping field $H_{\rm STOP}$. Point A denotes the demagnetized state of the system. Point B denotes the remanence state, with a remanent magnetization of $M_{\rm R}$.

reduced stopping field values will be designated as h_s. The data are then in the form of $m_{\rm IRM}(h_s)$ and $m_{\rm DCD}(h_s)$ profiles. In terms of these reduced parameters, $m_{\rm IRM}(h_s)$ will range from zero at $h_s = 0$ to one for large h_s, while $m_{\rm DCD}(h_s)$ will range from $+1$ at $h_s = 0$ to -1 for large h_s.

These reduced $m_{\rm IRM}(h_s)$ and $m_{\rm DCD}(h_s)$ profiles provide a basis for the analysis of the intergranular interactions in the system. From the Stoner–Wohlfarth model [10], a system with noninteracting uniaxial grains will satisfy the condition $m_{\rm IRM} = (1 - m_{\rm DCD})/2$ for any value of h_s. As discussed by Kelly *et al.* [16], if $m_{\rm IRM}$ is greater than $(1 - m_{\rm DCD})/2$ for a given h_s, this is an indication that the IG coupling is mainly due to exchange, while $(1 - m_{\rm DCD})/2 > m_{\rm IRM}$ indicates that magnetostatic coupling dominates. Reference [16] then uses a deviation parameter, $\Delta m = m_{\rm DCD} - (1 - 2m_{\rm IRM})$, as a measure of the type and relative strength of the IG interactions. A positive Δm means that exchange dominates the IG interactions and a negative Δm is an indication of magnetostatic dominance.

There are various ways in which one can use IRM and DCD data to determine the nature of the IG interactions. One can use individual Δm measurements, take the sign as indication of the type of interaction that is dominant and the magnitude as a measure of the strength of the interaction. Since Δm will depend on the stopping field, this approach does not provide a particularly good measure of the overall nature of the IG interactions.

This work takes a more integrated approach that takes the full $m_{\rm IRM}(h_s)$ and $m_{\rm DCD}(h_s)$ response into account. More specifically, the IRM and DCD remanence data will be analyzed on the basis of an interaction field model developed by Che and Bertram [11], and extended by Harrell *et al.* [12] and Huang *et al.* [13]. The summary below gives the basic operational equations. Full details can be found in [11]–[13].

In the Che–Bertram (CB) approach, one assumes a remanence dependent interaction field of the form

$$h_i(m_r) = \alpha m_r \tag{1}$$

where h_i is an effective interaction field normalized to the average switching field over the ensemble of particles, m_r can be either the reduced IRM or the reduced DCD remanence as defined above, and α is a dimensionless remanence mean field interaction parameter. With the average switching field taken as the coercive force, this field normalization convention is the same as introduced above. The field $h_i(m_r)$ is then taken as a measure of the mean-field IG interactions due to the exchange and/or the magnetostatic interactions. Insofar as exchange tends to line up grains, a positive α is an indication of exchange dominance. Based on the fact that dipole-dipole interactions tend to promote a lack of magnetization alignment from grain to grain, a negative value of α signifies magnetostatic dominance.

The second element of the Che–Bertram model of importance here is the assumption of an effective stopping field $h_{\rm se}$ that amounts to the *sum* of the experimental stopping field and the CB interaction field. In terms of the reduced field parameters used here, one can then write

$$h_{\rm se} = h_s + h_i(m_r). \tag{2}$$

Based on this assumption, one can make use of the full ensemble of IRM and DCD remanence versus stopping field data to obtain a determination of the CB $\alpha-$ parameter [12], [13]. This α can then be taken as a global measure of the IG interactions for the system.

As a graphical aid to a summary description of this α-extraction technique, consider the schematic diagrams in Fig. 2. The graphs show plots of $m_{\rm IRM}(h_s)$ and $[1 - m_{\rm DCD}(h_s)]/2$ versus the reduced stopping field h_s. Graphs (a) and (b) show schematic curves for cases when the IG interactions are dominated by exchange or magnetostatic interactions, respectively. The vertical axis will play an important role in the overall analysis and is taken to correspond to a remanence parameter u_r. Both $m_{\rm IRM}(h_s)$ and $[1 - m_{\rm DCD}(h_s)]/2$ share common limits of zero and one in the zero and large h_s limits, respectively. Both graphs show horizontal cuts (C) at fixed u_r, as indicated. The field intersection points of these cuts with the $m_{\rm IRM}(h_s)$ and $[1 - m_{\rm DCD}(h_s)]/2$ curves are labeled along the h_s-axis as $h_{\rm IRM}$ and $h_{\rm DCD}$, respectively. Following [12], it proves useful to define a field deviation parameter Δh according to

$$\Delta h = h_{\rm DCD} - h_{\rm IRM}. \tag{3}$$

A positive Δh is an indication of exchange dominance and a negative value implies that magnetostatic interactions dominate.

The key to the α-determination lies in the assumption that at cut C, the effective stopping field $h_{\rm se}$ is the *same* for both the IRM and DCD remanence states and that a nonzero Δh gives a direct measure of the difference in interaction fields for these two remanence processes. Based on this assumption, (2) and (3) combine to give

$$\Delta h = h_i(m_{\rm IRM}) - h_i(m_{\rm DCD}). \tag{4}$$

This is a key result. The Δh parameter represents more than the difference between two experimental stopping fields. It also represents the difference between the two interaction fields for the IRM and the DCD processes.

Finally, one can use the $h_i(m_r) = \alpha m_r$ condition from (1), replace $m_{\rm IRM}$ with u_r and $m_{\rm DCD}$ with $1 - 2u_r$, and obtain

$$\Delta h = \alpha(3u_r - 1). \tag{5}$$

If one now integrates both sides of (5) over the remanence parameter u_r, one immediately obtains a simple integral relation for α, namely

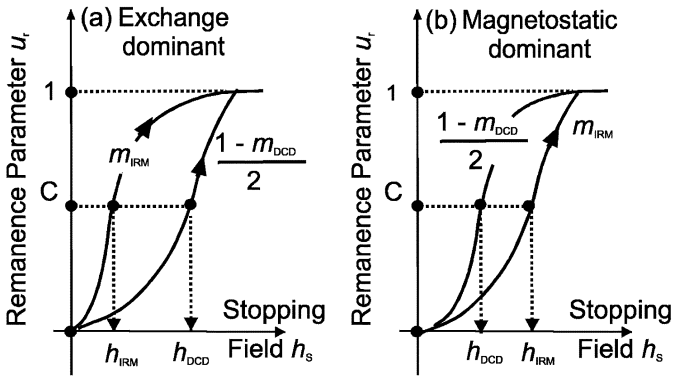

Fig. 2. Schematic remanence parameter versus reduced stopping field diagram that illustrates the isothermal remanence m_{IRM} and the modified demagnetization remanence $(1 - m_{\mathrm{MCD}})/2$ curves for a system with (a) exchange coupled grains and (b) dipolar coupled grains. The horizontal cut at constant μ_r labeled C in each diagram serves to define reduced stopping fields h_{IRM} and h_{DCD}, as indicated.

$$\alpha = 2 \int_0^1 \Delta h * du_r. \tag{6}$$

Note that the integral in (6) is also equal to the area between the $m_{\mathrm{IRM}}(h_s)$ and the $[1 - m_{\mathrm{DCD}}(h_s)]/2$ curves in either diagram of Fig. 2. For (a) the integral and the corresponding α will be positive and for (b) these quantities will be negative. Based on (6), then, the IRM and DCD remanence versus stopping field data and the area under curves of the sort shown in Fig. 2 can be used to obtain empirical values of the CB interaction parameter α. It is to be emphasized that this α value embodies the full ensemble of remanence data and not just values at a single stopping field.

The advantage of the effective field approach is that it can be extended to the study of IG interactions in soft magnetic thin films, where the magnetization reversal is due to domain wall pinning mechanisms. It is reasonable to assume that the pinning interaction fields remain the same during the IRM and DCD measurement processes. In consequence, the interpretation of the field deviation parameter Δh, and the CB interaction parameter α as indicative of the type and extent of IG interactions is also valid for soft magnetic thin films.

B. Dynamic Coercive Force and Effective Switching Volume

In the above IRM and DCD discussion, the coercive force from the standard static hysteresis loop was used as a convenient normalization parameter for the stopping field and the other fields in the analysis. It is important to keep in mind, however, that the coercive force actually exhibits a dependence on the time scale of the measurement process. For the situation at hand, the coercive force H_c is taken as the median of the switching field of an ensemble of magnetic particles, where the switching field of an individual particle is the externally applied field required to reverse the saturation direction. The origin of the dependence of H_c on the time scale of the measurement lies in the statistical nature of the switching event. The latter is a thermally assisted process that depends on the probability that the magnetic moment can cross an anisotropy based energy barrier and flip. An externally applied magnetic field serves to assist the reversal process by reducing the height of the effective energy barrier. This, in turn, allows the magnetic moment to switch on the time scale of interest. Consequently, the value of the external applied field required to switch the ensemble of particles decreases as one increases the time it is allowed to act. In other words, H_c will depend on the time t for which the external field is held. The time-dependent coercive force due to such a thermally assisted switching process is termed "dynamic coercive force."

Measurements of the dynamic coercive force, taken as $H_c(t)$, can be made in two ways. 1) Hysteresis loops may be recorded while the field is swept continuously at different rates. 2) Hysteresis loops may be recorded while the field is stepped instead of continuously swept. In the case of the continuously swept field, the field sweep rate defines the effective time scale for $H_c(t)$. In the case of the stepped field, the time scale is simply the waiting period after each field change and before the next measurement is made. For the purposes of this work, the stepped field approach was used to measure the $H_c(t)$. More details on the time scale dependence of the dynamic coercive force can be found in [14] and [15].

The standard way to quantify $H_c(t)$ data is through the model developed by Sharrock [14], [15]. The Sharrock $H_c(t)$ equation given below applies for two most commonly encountered situations: 1) when there is a misalignment of the external applied field with respect to the easy axis of a system of closely aligned uniaxial particles and 2) when there is a spread in the easy direction of a system of uniaxial particles. For these two situations, the Sharrock model gives a working equation of the form

$$H_c(t) = \frac{1}{2} H_k \left[1 - [2k_{\mathrm{B}}T/H_k M_s V) \ln(f_0 t)]^n\right]. \tag{7}$$

The leading H_k factor on the right-hand side denotes the uniaxial anisotropy field, k_{B} is Boltzmann's constant, T is the absolute temperature, M_s is the magnetization, V is the effective switching volume, f_0 is the attempt frequency for reversal, and n is a response exponent. The equation is given in Gaussian units. (7) quantifies the basic fact that the actual switching of a magnetic moment with a net value of $M_s V$ is thermally assisted, so that H_c can depend on time. The greater the temperature or the smaller the moment, the smaller the field that is needed on the average, to flip the moment from a direction opposite to the field to one along the field.

The right-hand-side combination of parameters in parenthesis in (7), $(2k_{\mathrm{B}}T/H_k M_s V)$, is simply the ratio of the thermal energy factor $k_{\mathrm{B}}T$ to the uniaxial anisotropy energy $H_k M_s V/2$. The inverse ratio, $(H_k M_s V/2)/k_{\mathrm{B}}T$, is often termed the thermal stability parameter, taken here as S. The larger S, the more stable a given anisotropic switching volume V will be against thermal fluctuations. The logarithmic $f_0 t$ factor reflects the statistical nature of the $H_c(t)$ response. The attempt frequency f_0 is typically taken at 1 GHz. For closely aligned uniaxial particles, but with a spread in the easy direction, the response exponent n is usually set to 0.7. These f_0 and n values will be used for the analysis in Section IV-B.

The Sharrock analysis can provide a useful formalism for the study of thermally assisted reversal processes in soft magnetic thin films. In this case, the barrier for thermal switching could be due to domain wall pinning sites. The activation energy

TABLE I
SUMMARY OF BASIC Fe–Ti–N FILM PROPERTIES AND PARAMETERS

Nitrogen content x_N (at. %)	Grain size[a] (nm)	Static coercive force H_c (Oe)	Static anisotropy field H_k (Oe)	Saturation induction $4\pi M_s$ (kG)
0.0	28	13.4	-	19.40
1.9	20	8.0	-	19.10
3.9	15	6.4	7.0	18.80
5.4	10	6.5	9.0	18.20
7.0	8.5	5.6	11.0	16.80
8.4	7.5	6.7	16.0	15.30
10.9	5	7.2	19.0	14.20

[a]Data on the grain size from Ref. 7.

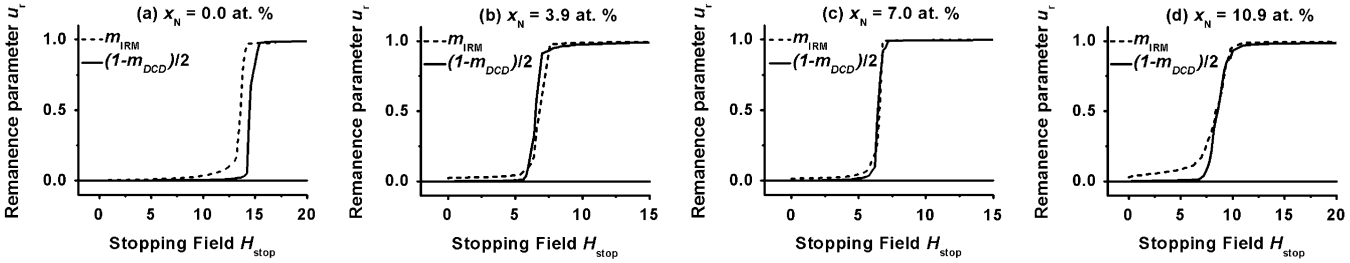

Fig. 3. Example IRM/DCD remanence parameter μ_r versus stopping field $H_{\rm Stop}$ profiles for Fe–Ti–N films with four different levels of nitrogen content (x_N), as indicated.

to overcome the pinning barrier also exhibits a dependence on the external applied field that is usually described by a power law, much in the same way as for nucleation dominated reversal processes. The thermal stability aspect of the present measurements followed a standard Sharrock approach. 1) The procedure outlined above was used to obtain $H_c(t)$ for the films. 2) Fits of the $H_c(t)$ response to (7) were then used to determine the anisotropy field H_k and thermal stability factor $S = 2k_{\rm B}T/H_kM_sV$. For a given film composition, M_s is known from static hysteresis loop measurements. The fitted S-values yield, therefore, estimates of the switching volume V. One would expect that grain interactions, regardless of the details, would result in a switching volume V that is somewhat larger than the volume of a single grain. However, as the results below will show, a standard Sharrock analysis of the Fe–Ti–N film data gives switching volumes with linear dimensions that are about 10–20 times larger than the known grain sizes.

III. Fe–Ti–N Thin Film Materials and Measurement Details

Magnetron sputtered Fe–Ti–N films with a common titanium content of about 3 at.% and nitrogen contents in the $0 \leq x_N \leq 10.9$ at.% range were used for the measurements. All films had nominal thicknesses in the 50 nm range. A magnetic field of 300 Oe was applied during the sputtering to produce a uniaxial in-plane anisotropy. Details on the film preparation and the materials analysis are given in [5] and [8]. Table I lists basic data on grain size [9], static coercive force, static uniaxial anisotropy field, and saturation induction for the films.

The basic magnetic characterizations and the remanence and dynamic coercive force measurements were done at nominal room temperature by standard superconducting quantum interference device (SQUID) magnetometry methods. For the IRM remanence measurements, the films were initially demagnetized in a dc external field. The remanence $M_{\rm IRM}$ was acquired at different values of the stopping field $H_{\rm stop}$ as described in Section II-A. The maximum value of $H_{\rm stop}$ was 100 Oe. For the DCD remanence measurements, the films were initially saturated in an external field of 100 Oe. The maximum value of $H_{\rm stop}$ used in this case was also 100 Oe. For both types of remanence measurements, $H_{\rm stop}$ was stepped by amounts that ranged from 0.2 Oe for fields near the center of the switching field distribution to 5 Oe for fields further away. The field $H_{\rm stop}$ was applied for 60 s and turned off, and the remanence was then measured after a further delay of 60 s. For the dynamic coercive force measurement, the hysteresis loop was traced as the external field was moved from $+100$ Oe to -100 Oe in 0.1 Oe steps for fields near the center of the switching field distribution. At each stepping point, the field was held for waiting times ranging from 1 to 500 s before the moment was measured. For both the remanence and dynamic coercive force measurements, the various field cycling operations around the static hysteresis loop and time delays were programmed to be done automatically.

The analysis procedures relevant to the data obtained from the IRM and DCD remanence measurements, and the dynamic coercive force measurements have been given in Section II. The extended CB model was used to extract the remanence field interaction parameter α as a function of the nitrogen content x_N.

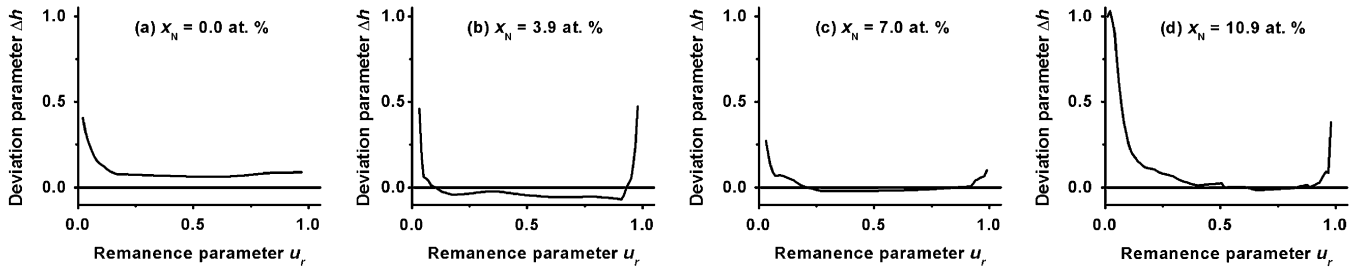

Fig. 4. Example IRM/DCD field deviation parameter Δh versus remanence parameter u_r profiles for Fe–Ti–N films with four different levels of nitrogen content (x_N), as indicated.

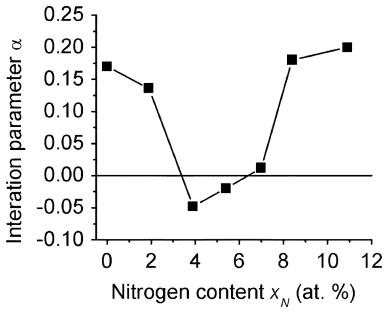

Fig. 5. Extracted remanence mean field interaction parameter α from the extended Che–Bertram analysis as a function of the nitrogen content X_N. As a guide to the eye, solid lines connect the data points.

Fits to the Sharrock dynamic coercive force model were used to obtain static H_k and thermal stability parameter S values, and to extract estimates of the switching volume V.

IV. Results and Discussion

A. Intergranular Interactions

Fig. 3 shows example data on the IRM/DCD remanence parameter u_r versus stopping field $H_{\rm stop}$ for four selected x_N values, as indicated. Fig. 4 shows data on the IRM/DCD field deviation parameter Δh vs. u_r for the same four x_N values. Recall that a positive Δh is an indication of exchange dominated IG interactions and a negative Δh indicates a predominance of dipole dipole interactions. The most interesting aspect of the graph panels in Fig. 4 is the clear differences in the Δh versus u_r profiles as one changes the level of the nitrogen in the films. For the end limits at $x_N = 0$, as in (a), and at $x_N = 10.9$ at.%, as in (d), the Δh values are mostly positive. For $x_N = 3.9$ at.%, as in (b), Δh is mostly negative, and for $x_N = 7.0$ at.%, as in (c), Δh is mostly zero. This indicates a clear change in the nature of the IG interactions for Fe–Ti–N films with nitrogen content.

Recall also from the CB interaction field analysis, that the area under the Δh versus u_r curve corresponds to one half the remanence mean field interaction parameter α. Fig. 5 shows α as a function of x_N, with all values extracted from area under the curve determinations from plots of the sort shown in Fig. 4. The $\alpha(x_N)$ results in Fig. 5 quantify the trends noted from the Δh versus u_r profiles in Fig. 4. One sees that for low nitrogen values, typically below 4 at.% or so, the α parameter is large and positive, an indication that exchange dominates the IG interactions. In the range 4 at.% $< x_N <$ 7 at.%, one can see that α becomes slightly negative. This is an indication that there is a weak trend toward dipole–dipole dominance in the IG interactions. Finally, for $x_N > 7.0$ at.%, α moves back into the large and positive regime and exchange dominance.

This intriguing evolution from a strong exchange dominated IG interaction for low x_N values, to a region with weak dipole-dipole dominance at intermediate nitrogen levels, and finally to a return to exchange dominance at large x_N values can be qualitatively explained in terms of two effects: 1) the decrease in grain size with increasing nitrogen content and 2) the eventual drop in the grain size below the exchange length for x_N values above 7 at.%. The proposed scenario is as follows. First, as x_N increases from zero to about 4 at.%, the decrease in grain size is accompanied by the creation of more and more voids and grain boundaries. This, in turn, results in an increase in the intergranular dipolar interactions at the expense of exchange coupling and there is a gradual downturn in the α versus x_N response. The zero crossing from positive to negative α values at $x_N \approx$ 4 at.% is an indication that the exchange dominated IG interactions in the large grain, low nitrogen limit have been ameliorated by the grain boundary and void development, so that the weaker magnetostatic interactions become dominant. The data indicate that the magnetostatic interactions remain dominant as long as the grain size remains larger than the exchange length. As x_N moves above about 7 at. %, for which the grain size falls below the exchange length, one sees a relatively sharp upturn in the α versus x_N, a second zero crossing, and a return to large and positive α values. The second crossover and return to large α values provides a clear demonstration of the role of the exchange length *vis a vis* the grain size in remanence processes.

B. Thermal Stability and Inferred Switching Volume

Results on the dynamic coercive force as a function of the field holding time for the three samples with the largest x_N values are shown in Fig. 6. For films with lower nitrogen levels, the change in the coercive force as a function of the field holding time was within experimental error due to which no meaningful information could be extracted. This is due to the large grain size and the corresponding large associated switching volumes in these films which lead to very large thermal stability factors and very small changes in $H_c(t)$. In Fig. 6, the data are shown by the solid circles and indicated error bars. The Sharrock fits are shown by the solid curves, with the different values of the anisotropy field H_k and the thermal stability parameter $S = 2k_{\rm B}T/H_kM_sV$, as indicated. Recall that all fits are based on f_0- and n-values of 1 GHz and 0.7, respectively. Table II

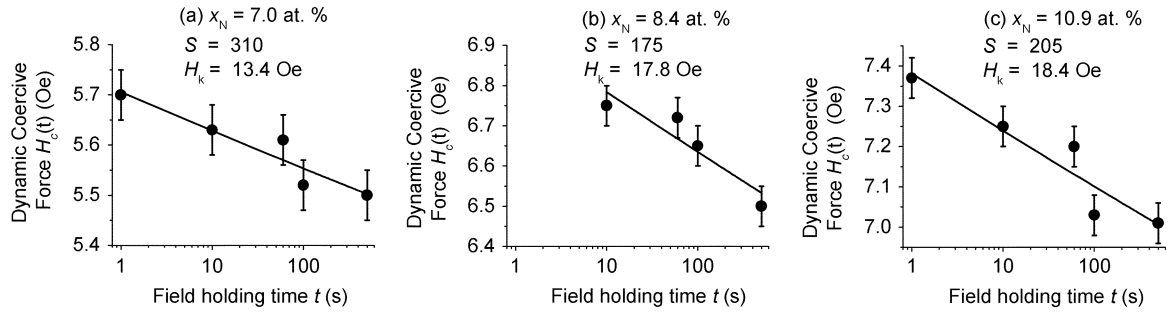

Fig. 6. Data and Sharrock equation fits for the dynamic coercive force $H_c(t)$ as a function of the field holding time t for the three films with the highest levels of nitrogen (X_N), as indicated. The solid circles show the data. The solid curves show the fits. The values of the thermal stability parameter S and the anisotropy field parameter H_k needed to obtain the fits shown are also as indicated.

TABLE II
SUMMARY OF SHARROCK MODEL FIT PARAMETERS AND COMPARISON GRAIN SIZE PARAMETERS

Nitrogen content x_N (at. %)	Thermal stability parameter [a] $H_k M_s V/2k_BT$	Anisotropy field parameter [a] H_k (Oe)	Effective switching volume [b] V (cm^3)	Effective switching volume dimension $V^{1/3}$ (nm)	Grain size [c] a (nm)
7.0	310 ± 72	13.4 ± 0.4	1.4×10^{-15}	113	8.5
8.4	175 ± 53	17.8 ± 1.2	6.7×10^{-16}	87	7.5
10.9	205 ± 45	18.4 ± 0.8	8.2×10^{-16}	93	5

[a]Sharrock optimal fit parameters to the dynamic coercivity data in Fig. 6.
[b]Calculated from the optimal fit parameters to the dynamic coercivity data in Fig. 6.
[c]From the grain size determination given in [7].

lists these same H_k and S-values, along with inferred values of the effective switching volume V, the corresponding length parameter $V^{1/3}$, and the relevant grain size a-values from Table I. The conversions from S to V were based on the H_k optimal fit values determined above and the $4\pi M_s$ values listed in Table I.

The three graphs in Fig. 6 all show the expected decrease in the dynamic coercive force with the field holding time. The physics behind the drop lies in the time scale of the usual thermally activated magnetization and demagnetization processes that control the shape of the hysteresis loop. When the time scale of the field steps is short, the magnetization is unable to respond quasistatically, and one sees an anomalously large coercive force. As the time scale of the field steps is extended, the entire loop as well as the coercive force approaches the response one expects in the quasi-static limit. The fits to the Sharrock model yields semiquantitative estimates of the thermal stability parameter S as well as the effective switching volume V. The fits shown in Fig. 6 demonstrate a reasonable trend. One can see that as x_N increases from 7.0 at.% to 10.9 at.%, the S-parameter tends to decrease. In general, the calculated unit switching volume V also decreases as x_N increases and the grain size decreases. The small increase in the S-parameter and the unit switching volume V as x_N increases above 8.4 at.% is suggestive of an overlap in the distribution of the grain size for these films. The change in the thermal stability factor could also be due, in part, to a grain size related change in the switching energy barriers with x_N. The decrease in grain size with increasing x_N could lead to decreased domain pinning energies and decreased thermal stability factors.

The uniaxial anisotropy field parameters estimated from the Sharrock analysis of the dynamic coercive force are in reasonable agreement with the values calculated from the static hysteresis loop measurements. The linear dimension of a switching unit is however, about 10–20 larger than the size of an individual grain. When grains interact, the volume of a switching unit is expected to be somewhat larger than the volume of an individual grain. It is speculated that for soft magnetic systems such as these Fe–Ti–N films, the large value of the saturation induction coupled with the nanoscale dimension of the grains leads to strong IG magnetostatic interactions that are spread over many grains. In such a case, the effective switching volume can be considerably larger than the grain volume. On the other hand, strong IG exchange interactions can also lead to large effective switching volumes, as is the case in the Fe–Ti–N films with x_N above 8 at.%. The picture is however, less clear when the exchange and magnetostatic interactions tend to cancel each other, as in the films with x_N in the 6–8 at.% range. In these films, the reason for the large difference between the effective switching volume and the grain volume is not well understood at present.

V. CONCLUSION

The intergranular interactions and thermal stability in Fe–Ti–N thin films have been investigated as a function of the nitrogen content. The intergranular interactions were analyzed on the basis of an interaction field analysis technique, and the thermal stability was analyzed from the Sharrock model of the dynamic coercive force. The change in the type and strength of the interactions, and in the thermal stability factors can be

explained by the change in the grain size with the nitrogen content. The linear dimension of a switching unit is about 10–20 times larger than the size of a grain.

ACKNOWLEDGMENT

This work was supported in part by the Information Storage Industry Consortium (INSIC) Extremely High Density Recording (EHDR) program, the U.S. Office of Naval Research under Grant N00014-06-0889, and the U.S. Army Research Office under Grant W911NF-04-1-0247.

Dr. Y. Ding and Prof. C. Alexander, Jr. of the University of Alabama, Tuscaloosa MINT Center kindly prepared and provided the Fe–Ti–N films for this work, as well as materials characterization data and many useful discussions.

REFERENCES

[1] H. Y. Wang, Y. J. He, Z. W. Ma, E. Y. Jiang, H. S. Huang, and W. H. Mao, "High moment soft magnetic FeTiN thin films for magnetic recording head materials," *J. Appl. Phys.*, vol. 85, pp. 3745–3748, 1999.

[2] S. C. Byeon, Y. Ding, and C. Alexander, Jr., "High moment FeTiN thin films for high density recording heads," *IEEE Trans. Magn.*, vol. 36, no. 5, pp. 2502–2505, Sep. 2000.

[3] Y. V. Khivintsev, B. J. Kuanr, I. Harward, R. E. Camley, and Z. Celinski, "Iron-based microstrip band-stop filters at higher microwave frequency range: Design optimization using shape anisotropy," *J. Appl. Phys.*, vol. 99, p. 08P512 1–3, 2006.

[4] B. K. Kuanr, D. L. Marvin, T. M. Christenson, R. E. Camley, and Z. Celinski, "High-frequency magnetic microstrip local bandpass filters," *Appl. Phys. Lett.*, vol. 87, pp. 222506–222508, 2005.

[5] Y. Ding, S. C. Byeon, and C. Alexander, Jr., "Role of nitrogen concentration in the thermal stability of the anisotropy in FeTiN thin films," *IEEE Trans. Magn.*, vol. 37, no. 4, pp. 1776–1778, Jul. 2001.

[6] A. V. Mijiritskii and D. O. Boerma, "Phase transformations in epitaxial Ni/Fe bilayers upon low-temperature gaseous nitriding," *Phys. Rev. B*, vol. 64, pp. 035410–035421, 2001.

[7] Y. Ding and C. Alexander, Jr., "Distribution of nitrogen atoms inside epitaxial (110) FeTiN films," *J. Appl. Phys.*, vol. 91, pp. 7833–7835, 2002.

[8] J. O. Rantschler, Y. Ding, S. C. Byeon, and C. Alexander, Jr., "Microstructure and damping in FeTiN and CoFe films," *J. Appl. Phys.*, vol. 93, pp. 6671–6673, 2003.

[9] J. O. Rantschler, "Ferromagnetic resonance and microstructure of soft magnetic thin films," Ph.D. dissertation, Univ. Alabama, Tuscaloosa, 2003.

[10] E. P. Wohlfarth, "Relations between different modes of acquisition of the remanent magnetization of ferromagnetic particles," *J. Appl. Phys.*, vol. 29, pp. 595–596, 1958.

[11] X. Che and H. N. Bertram, "Phenomenology of δ M curves and magnetic interactions," *J. Magn. Magn. Mater.*, vol. 116, pp. 121–127, 1992.

[12] J. W. Harrell, D. Richards, and M. R. Parker, "Delta-H plot evaluation of remanence behavior in barium ferrite tapes and disks," *J. Appl. Phys.*, vol. 73, pp. 6722–6724, 1993.

[13] P. Huang, J. W. Harrell, M. R. Parker, and K. E. Johnson, "Interaction fields and media noise in CoPtCr thin films," *IEEE Trans. Magn.*, vol. 30, no. 6, pp. 4002–4004, Nov. 1994.

[14] M. P. Sharrock, "Time dependence of switching fields in magnetic recording media," *J. Appl. Phys.*, vol. 76, pp. 6413–6418, 1994.

[15] M. P. Sharrock, "Measurement and interpretation of magnetic time effects in recording media," *IEEE Trans. Magn.*, vol. 35, no. 6, pp. 4414–4422, Nov. 1999.

[16] P. E. Kelly, K. O'Grady, P. I. Mayo, and R. W. Chantrell, "Switching mechanisms in cobalt-phosphorus thin films," *IEEE Trans. Magn.*, vol. 25, no. 5, pp. 3881–3883, Sep. 1989.

Manuscript received November 2, 2006; revised May 16, 2007. Corresponding author: K. Srinivasan (e-mail: Kumar_S@dsi.a-star.edu.sg).